Averrhoa bilimbi leaves-derived oxygen doped 3D-linked hierarchical porous carbon as high-quality electrode material for symmetric supercapacitor

by Rika Taslim

Submission date: 13-Apr-2023 01:58PM (UTC+0700)
Submission ID: 2063286411
File name: 13._Belimbing_Journal_of_Energy_Storage_52_2022_104911.pdf (2.99M)
Word count: 10971
Character count: 59420

Journal of Energy Storage 52 (2022) 104911

Contents lists available at ScienceDirect

Journal of Energy Storage

journal homepage: www.elsevier.com/locate/est

Research papers

Averrhoa bilimbi leaves-derived oxygen doped 3D-linked hierarchical porous carbon as high-quality electrode material for symmetric supercapacitor

Erman Taer [a,*], Apriwandi Apriwandi [a], Nursyafni Nursyafni [a], Rika Taslim [b]

[a] Department of Physics, Faculty of Mathematic and Natural Sciences, University of Riau, Simpang Baru, Pekanbaru, Indonesia
[b] Department of Industrial Engineering, State Islamic University of Sultan Syarif Kasim, Simpang Baru, Riau, Indonesia

ARTICLE INFO

Keywords:
Oxygen doped
Activated carbon
Averrhoa bilimbi leaves
Electrode materials
Supercapacitor

ABSTRACT

This successfully performed a facile one-way KOH impregnation strategy, to hierarchically prepare interconnected porous carbon and self-oxygen doped from *Averrhoa bilimbi* leaves waste, as binder-free electrode material (PCBLs) for high-quality symmetrical supercapacitor. 3D porous structure and surface area PCBLs-derived controlled by different KOH concentrated solution. KOH infiltrated into precursor as act activation agent to completely removed inorganic impurities, result high carbon content of 85.54–87.22% with oxygen functional group of 10.61–14.71%. The precursor impregnated at 0.5 mol/L possessed excellent micropores 87.69%, adjusting mesopores and appropriate amounts of oxygen doped of 14.71%. As a result, it performed high performance of symmetrical supercapacitor. Furthermore, the electrochemical performance was evaluated within a two-electrode system using a binder-free solid coin design in different aqueous electrolytes of 1 M H_2SO_4, NaOH, and Na_2SO_4, respectively. This indicated that the symmetric supercapacitor-based PCBL-5 had a high specific capacitance of 293 F g^{-1} in 1 M H_2SO_4 aqueous electrolyte at a current density of 1.0 A g^{-1}. It also showed impressive energy densities of 26.54, 21.85, and 16.12 Wh kg^{-1} in 1 M H_2SO_4, NaOH, and Na_2SO_4, at an optimum power density of 178.44 W kg^{-1}. The observed desirable excellent material and electrochemical behaviors of the new source hierarchical porous carbon derived from *Averrhoa bilimbi* leaves waste would be a competitive candidate as electrode material in the development of high-quality supercapacitor devices.

1. Introduction

Energy conversion systems and storage devices are important aspects that should encourage the creation of effective, efficient, sustainable, renewable, and pollution-free green power sources. As an alternative device, supercapacitors are found to combine the advantages of energy storage systems, including traditional capacitors and batteries [1]. This indicates that supercapacitor is an efficient, clean, safe, and cheap alternative energy storage device, which provides high power and fast charging rate, as well as possess a very long life cycle [2]. Due to their high performances, these devices have reportedly been applied to electric vehicle technology, communication and pulsed laser systems, as well as military equipment, although low energy output limits their practical applications [3]. The energy storage capacity of the supercapacitor depends on the charge accumulation at the EDLC (electrode/electrolyte interface) or the rapidly reversible redox reaction between the electrolyte and the surface heteroatom functional groups, as a pseudo-capacitance behavior [4]. This indicates that electrode modification with 3D hierarchical interconnected and controlled pore structures is the main key to enhancing supercapacitor energy, accompanied by electrolytic ion variations [5–7]. In addition, the electrode materials providing hierarchical 3D pores with a high surface area includes metal oxides/hydroxides [8], transition metal sulfides [9], conductive polymers [10], metal-organic frameworks [11], and porous carbon [3].

Recently, porous carbon has recently displayed outstanding material properties as a high-performance electrode material, especially in biomass-based activated carbon with a specific surface area of ~4000 m^2 g^{-1} [12,13]. This is also in accordance with a newly study reported by Jiang et al. [14] which confirms the potential of the plant as an advanced material electrode for supercapacitor [14]. Despite the relatively low mean capacitive properties of 200 F g^{-1}, these materials have been successfully synthesized through a clean, inexpensive, non-toxic,

* Corresponding author.
E-mail address: erman.taer@lecturer.unri.ac.id (E. Taer).

https://doi.org/10.1016/j.est.2022.104911
Received 2 March 2022; Received in revised form 28 April 2022; Accepted 14 May 2022
Available online 23 May 2022

and corrosive-free facile approach, compared to metal oxides, conducting polymers, and metal-organic frameworks. Several previously reported biomass conversion strategies into porous activated carbon have been found to be effective, such as hydrothermal [14], chemical-physical activation [15], molten salt [16], and template [17]. Among these techniques, the chemical-physical activation method is mostly recommended, due to being simpler, easier, more cost-effective, and time-saving [18]. Moreover, the porous structures obtained is interestingly a hierarchical 3D adjustable pore and self-doping heteroatoms, such as N, O, P, which ensures high EDLC properties and the apparent pseudo-capacitance possessed by activated carbon-based electrode materials [19–21]. According to Aruchamy et al. [22], porous carbon was obtained from *Parthenium hysterophorous* leaves, through the chemical activation of KOH with ultra-high surface area of 4014 $m^2 g^{-1}$ [22]. This indicated that the supercapacitor electrode obtained a high specific capacitance of 270 F g^{-1} and a confirmed oxygen doped heteroatom of 6.35%. The study of Zheng et al. [22] also synthesized activated carbon from kapok flower, through the impregnation of 4:1 KOH:carbon, indicating the abundance of oxygen doped as a supercapacitor electrode, which improved the specific capacitance of 286 F g^{-1} [23]. Based on Zhang et al. [24] adjustable micro and macropore ratios of biomass-based activated carbon were provided for the performance of outstanding capacitive properties. This indicated an excellent specific capacitance of 477 F g^{-1} in an aqueous electrolyte, regarding a pecan shell waste-based activated carbon electrode [24]. In addition, Xu et al. [25] modified an electrode based on the activated carbon obtained from honeysuckle flowers, to suit a liquid ionic electrolyte through KOH impregnation, subsequently leading to a capacitive property of 186 F g^{-1} [25]. Although the obtained energy density was mostly between 10 and 20 Wh kg^{-1} with a relatively low conductivity, these studies were still found to be very interesting. This was because very few biomass precursors were synthesized by the best approach to generate 3D-linked hierarchical pore structures, accompanied by heteroatom self-doping. Therefore, the development of activated carbon-based electrode materials from new biomass precursors is still a big challenge to increase the energy density of supercapacitors. This indicates that there has been no study on starfruit (*Averrhoa bilimbi* L.) leaves waste as a carbon material with a 3D hierarchical pore structure with self-heteroatoms doped. *Averrhoa bilimbi* is a tropical fruit originating from Malaysia, which is subsequently distributed to Indonesia, Singapore, Thailand, and other Southeast Asian countries [26]. In Indonesia, it is also one of the leading agricultural commodities with high production of 101,553 tons/year [26]. Based on the continuous yearly harvest period, the dried leaves of this fruit assumably cause high waste and pollution. Recent studies have reported a high potential of dried starfruit leaves as activated carbon as electrode material [27,28]. However, their applications as supercapacitors are relatively low and should be deeply investigated.

Based on the aforementioned conditions, this study aims to determine a 3D-linked hierarchical porous carbon followed by self-oxygen doped was synthesized and optimized from starfruit (*Averrhoa bilimbi* L.) leaves effluent via one-way KOH impregnation as a high-quality electrode material (PCBLs). The obtained activated carbon was prepared for electrochemical evaluation in a two-electrode configuration system, through a binder-free design. Subsequently, the precursor was converted through a combination of pre-carbonization, KOH impregnation, carbonization, and physical activation. This indicated that the pore structure distributions were controlled by different KOH impregnation concentrations, at 0.3, 0.5, and 0.7 mol/L, respectively. To confirm their best electrochemical properties, the PCBLs electrodes were reviewed in different 1 M aqueous electrolytes, including H_2SO_4, NaOH, and Na_2SO_4. Using a facile, simple, clean, and cost-effective method, the presented leaves waste-based porous carbon demonstrated good electrode supercapacitors application, with its advantages indicating the following, (i) The chemical impregnation of KOH at different concentrations controlled 3D hierarchical pores and self-oxygen doped, and (ii) the binder-free electrode design ensured high conductivity in supercapacitor applications, through a two-electrode configuration. Therefore, this work highlights the potential of starfruit (*Averrhoa bilimbi* L.) leaves as a source of hierarchical porous carbon rich in self-oxygen doped for high-quality electrode materials in energy storage device applications.

2. Materials and methods

2.1. Precursor and material preparation

Green *Averrhoa bilimbi* leaves were harvested from the farm of the University of Riau, Pekanbaru, Indonesia, and sundried until the color became pale. Subsequently, the precursor was sliced into small pieces and heated through a drying oven at 110 °C. The sample was then pre-carbonized through a vacuum oven at 250 °C, as well as ground using a ball-milling and crusher via a 250 mesh sieve. At <60 μm, the homogeneous powder samples were ready to be chemically impregnated and converted to a monolithic solid coin precursor. In this study, the utilized chemicals include KOH, NaOH, H_2SO_4, and Na_2SO_4, obtained from Merck KgaA, Darmstadt, Germany, and Qui Mica S.A.U, Barcelona, Espana. KOH was used with a precursor as a chemical impregnation, while NaOH, Na_2SO_4, and H_2SO_4 were utilized as aqueous electrolytes.

2.2. Porous carbon Averrhoa bilimbi leaves (PCBLs) preparation

The chemical impregnation of KOH solution with precursor powder was performed through a hotplate at 5:1. This indicated that approximately 150 mL of KOH solution was prepared in a beaker and mixed with 30 g of precursor powder. Subsequently, the mixture was placed on a hotplate weistirer and rotated at 80 °C and 300 rpm, respectively. In this study, the KOH solution was varied at four different concentrations, including 0.0, 0.3, 0.5 and 0.7 mol/L, where the chemically-impregnated precursor was dried in a drying oven at 110 °C for 36 h. The powder obtained was then milled and converted into a 20 mm diameter coin solid through a 250 mesh sieve and hydraulic press, respectively. The impregnated precursor powder was also prepared to weigh 0.7 g and subsequently placed in a metal mould with a diameter of 20 mm. Furthermore, the container was compressed through a hydraulic press at a pressure equivalent to a mass of 8 tons, although did not require any binder. For each KOH concentration variation, as many as 20 pieces of solid coin precursors were prepared and placed in horizontal furnace tubes for high-temperature pyrolysis. In this study, the pyrolytic process contained carbonization and physical activation, which were carried out in one integrated step. This indicated that carbonization was carried out by continuously flowing N_2 gas into the furnace tube from 30–289 °C and 299–600 °C, at gas rates of 1 and 3 °C/min, respectively. The physical activation process was also marked by the change of the furnace atmosphere from N_2 to CO_2 at 600 °C. This was subsequently increased to 800 °C at 10 °C/min for 2 h 30 min. Additionally, the solid carbon of the obtained coins was neutralized by washing with distilled water for 4–5 days, until the ABLs were neutral (pH = 7). To facilitate data interpretation, the samples were denoted as PCBL–P, PCBL–3, PCBL–5, and PCBL–7, respectively. The preparation of PCBLs as high-quality electrode material for symmetric supercapacitor was reviewed in Scheme 1.

2.3. Material characterizations

The change in the density of the carbon coin PCBLs was evaluated through the shrinkage of dimensions on high-temperature pyrolysis. This indicated that density was calculated based on the standard equation of solid coin mass, thickness, and diameter, with the design being assumed to have the shape of cylinder geometry [29]. The morphological properties and porosity of PCBLs were also reviewed by scanning electron microscopy (SEM) and N_2 gas absorption, where the specific surface area (SSA) was analyzed using the Brunauer–Emmett–Teller

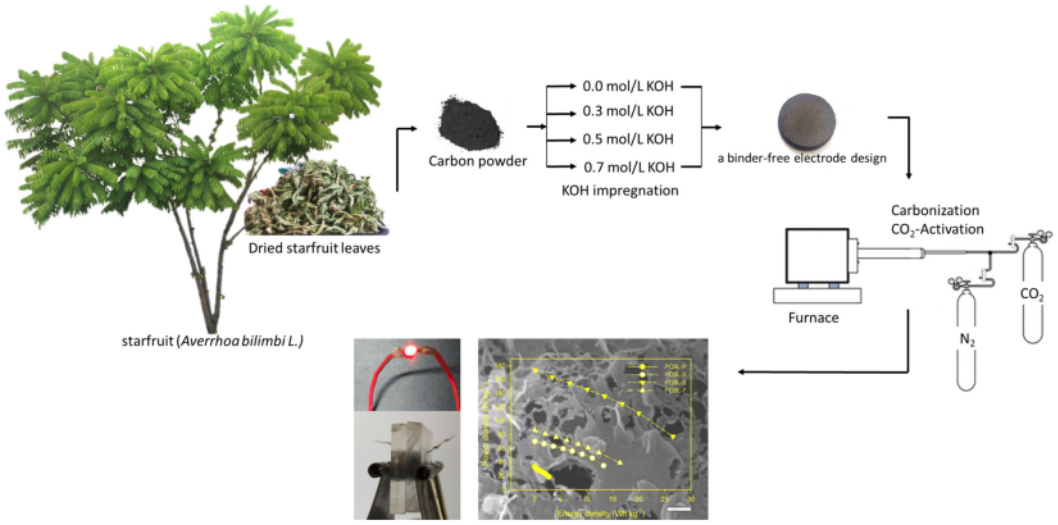

Scheme 1. The preparation of PCBLs as high-quality electrode material for symmetric supercapacitor

(BET) method. Subsequently, the pore size distribution was assessed using the Barrett–Joyner–Halenda (BJH) and non-local density functional theory (NL–DFT) techniques. In this study, the phase structure and functional group groups were detected by X-ray diffraction (XRD) and Fourier transform infra-red (FTIR). Lattice parameters such as interlayer spacing (d_{hkl}) and microcrystalline dimensions ($L_{c/a}$), were also evaluated by Bragg's law and the Debye–Scherrer equation, with the elemental status of the carbon PCBLs being reviewed through the energy dispersive spectroscopy (EDS) method.

2.4. Electrochemical performances

The electrochemical properties of supercapacitors were evaluated through cyclic voltammetry (CV), galvanostatic charge/discharge (GCD), and electrochemical impedance spectroscopy (EIS) methods. This was carried out in different aqueous electrolytes within a two-electrode configuration system, namely 1 M H_2SO_4, NaOH, and Na_2SO_4. The working electrode was also prepared by a binder-free solid coin design, with a diameter and thickness of 8 and ±0.2 mm, respectively. Moreover, a supercapacitor cell separator was prepared from an eggshell membrane at a 0.5 mm thickness, with CV and GCD were assessed within 0.0–1.0 V at different scan rates and constant current density of 1–10 mV s^{-1} and 1.0 A g^{-1}, respectively. Electrochemical impedance spectroscopy was also evaluated from 10 MHz to 100 kHz, with the specific capacitance, as well as energy and power densities being determined by standard equations based on a two-electrode system.

3. Results and discussions

Biomass-based porous activated carbon had great potential in designing solid binder-free electrode materials, as reported by previous studies. This approach specifically benefitted the materials in maintaining high real electrochemical conductivity. Furthermore, the *Averrhoa bilimbi* leaves-based porous activated carbons showed similar potency and should be initially evaluated on the effect of high-temperature pyrolysis. Fig. 1 illustrates the densities of the designed PCBLs in a solid system electrode material, where the selected treatment including KOH impregnation, carbonization, and physical activation, significantly affected the design dimensions. Before the integration of one-step carbonization and physical activation, the density of PCBLs was

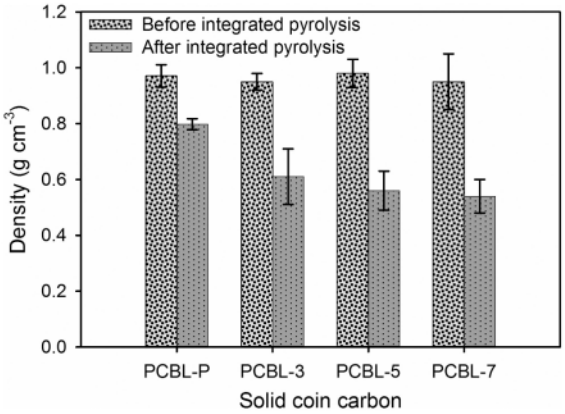

Fig. 1. The density reduction of PCBLs.

approximately 0.998 g cm^{-3} at a measurement error of 2.45%. After the application of several treatments, the solid dimensions of the PCBLs coins regularly decreased to 0.7980, 0.6100, 0.5600, and 0.5400 g cm^{-3} for PCBL-P, PCBL-3, PCBL-5, and PCBL-7, respectively. This indicated that the impregnation of KOH solution with 0.0–0.7 mol/L graded concentration had a higher density reduction of approximately 45.89% at high-temperature pyrolysis. The result subsequently initiated the evaporation and formation of the complex compound and carbon cavity structure in the solid PCBLs. Increasing the concentration of KOH also ensured more carbon reactions, where the byproducts produced K_2CO_3 and repeatedly reacted with C to produce evaporated CO_2 and CO compounds [30]. Moreover, the physical activation temperature of 800 °C maximized the reduction of tar and ash in the precursor material, allowing the opening of small pores and increasing the formation space of a high carbon framework [31,32]. The combination of these two processes subsequently initiated the formation of high porosity, characterized by their decreased density. However, the <50% density shrinkage still maintained their solid form strength for increased conductivity and porosity properties. This was analyzed more deeply on the pore structure and morphology, through SEM and N_2 gas absorptions, as well as the electrochemical property analyses.

Based on this study, the stratified synthetic route of KOH chemical impregnation, carbonization, and physical activation of the PCBLs improved their morphological structure and porosity, as shown in Figs. 2 and 3. To increase their SSA, the impregnation process was used to create a hierarchical porous network on the carbon surface, where the morphology of the obtained PCBLs samples was evaluated by SEM (Fig. 2a–h). This indicated that the PCBL-P obtained without KOH impregnation morphology showed carbon block aggregates (Fig. 2a), due to being generally smooth with no obvious porous framework signs (Fig. 2b). In addition, there was a large pore of 292 nm in the 50 nm magnification area, where the obtained PCBL-3 relatively showed different morphologies indicating a confirmed framework, although they were not markedly visible (Fig. 2c). This indicated that the impregnation of 0.3 mol/L KOH caused the formation of carbon walls, subsequently initiating 3D hierarchical pores. Also, Fig. 2d had mesopores between 10 and 25 nm, with the area at 50 nm magnification showing their hierarchical structure with an abundance of micropores. This indicated that the reaction of KOH with the precursor carbon discharged the complex bonds of the carbon wall as CO, CO_2, and H_2O, which initiated the formation of the mesopores and rich micropores [33,34], as shown in Table 1. At higher concentrations in PCBL-5, KOH impregnation intensely reduced the carbon frameworks, leading to their hierarchical structure formation being optimum all over the surface (Fig. 2e–f). This pore characteristic essentially ensured high ion exchange, with increased electro-active current providing great power for the electrode material [35,36]. The holes within the walls of the pores also allowed the 3D movement of the ions across all possible active surfaces, leading to multiple electrical layers and increased energy density [37], as shown in the CV and GCD profiles. According to the prepared magnification area, macropores and mesopores were detected between 115–204 nm and 16–45 nm, respectively. At high KOH concentration, the increase within the PCBL-7 also showed all-surface pore morphology with various sizes on the nm to micron scale, as presented in Fig. 2g. Due to the larger KOH impregnation, the carbon skeleton erosion initiated the new pores formation and the expansion of their diameter size, with the macro and mesopores ranging between 67–345 nm and 24–49 nm, respectively. In addition, no 3D pores structures were found on the PCBL-7 as shown by the 50 nm zoom, indicating that the provision of higher KOH concentrations eroded the carbon frameworks and reduced their 3D porous structure.

The porosity characteristics and comprehensive pore information of the PCBLs were also determined using the nitrogen adsorption-desorption measurements at a temperature of 77 K. This indicated that the PCBLs showed different nitrogen adsorption-desorption profiles, as illustrated in Fig. 3, where PCBL-P exhibited a type-III feature uncommon for porous carbon, subsequently confirming very weak porosity. The open hysteresis loops also characterized imperfect mesoporous structures with widened pores in the middle, compared to the top

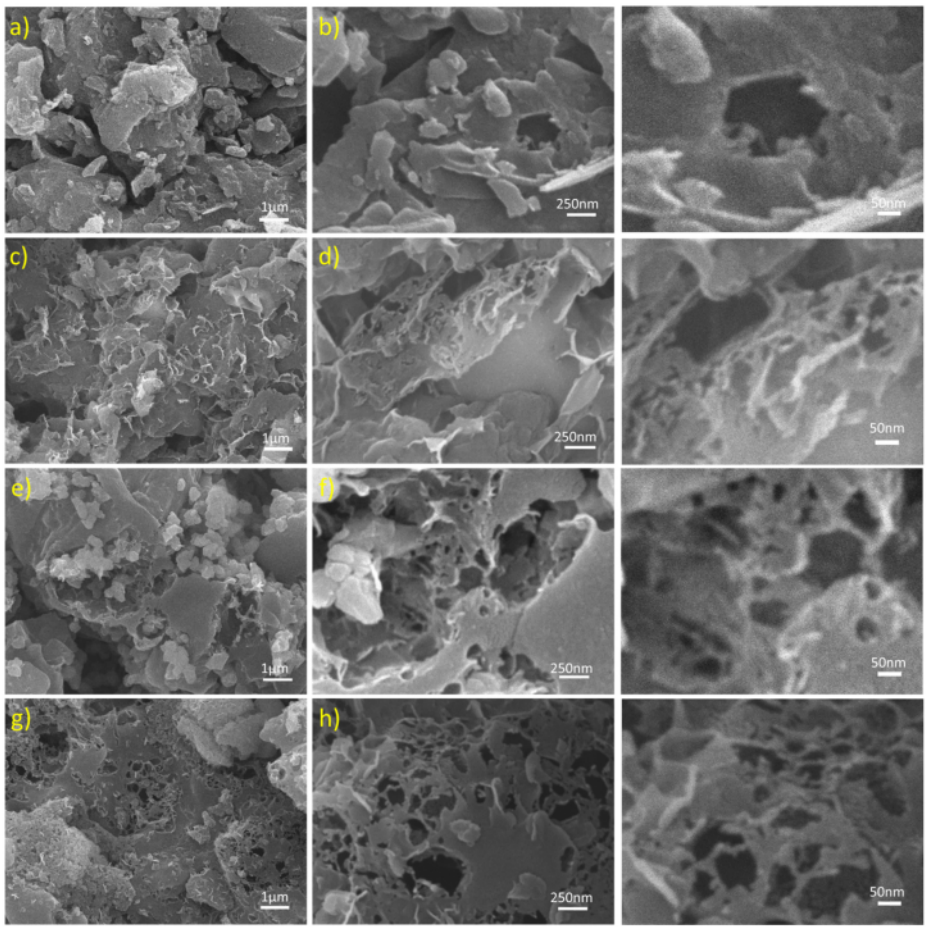

Fig. 2. SEM image of PCBL-P at (a) 1 μm, (b) 250 nm, PCBL-3 at (c) 1 μm, (d) 250 nm, PCBL-5 at (e) 1 μm, (f) 250 nm, and PCBL-7 at (g) 1 μm, (h) 250 nm.

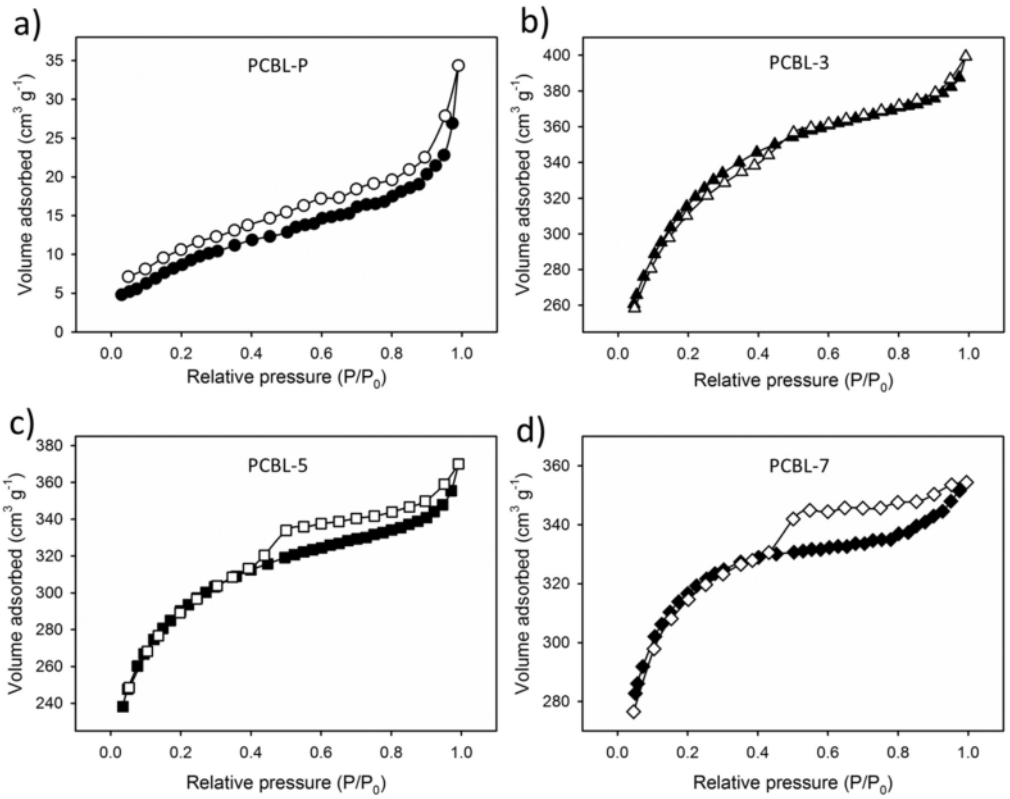

Fig. 3. Nitrogen adsorption–desorption isotherms of (a) PCBL-P, (b) PCBL-3, (c) PCBL-5, and (d) PCBL-7.

Table 1
Porosity properties of PCBLs.

PCBLs	S_{BET} (m^2 g^{-1})	S_{mic} (m^2 g^{-1})	S_{meso} (m^2 g^{-1})	V_{tot} (cm^3 g^{-1})	D_{aver} (nm)
PCBL-P	35.500	19.044	16.956	0.0531	5.9
PCBL-3	992.360	757.455	234.904	0.6177	2.4
PCBL-5	936.086	820.863	115.223	0.5725	2.5
PCBL-7	900.809	697.964	202.846	0.5482	2.3

(Fig. 3a). According to Table 1, PCBL-P had a surface area and volume of 35.5 m^2 g^{-1} and 0.0531 cm^3 g^{-1}, respectively. At different concentrations in high-temperature pyrolysis, the KOH activation significantly showed a characteristic IV-type curve, which was very different from PCBL-P (Fig. 3b–d). In addition, a large increase at a low relative pressure of P/P0 < 0.1 indicated rich microporosity, while a hysteresis loop at 0.4 < P/P0 < 1.0 signified highly developed mesoporosity. In this study, an increase in absorption also indicated macroporosity at a relative pressure greater than 0.95. This showed that the KOH impregnation on the biomass precursor of *Averrhoa bilimbi* leaves obtained a hierarchical pore structure with high porosity, as discussed previously in the SEM image (Fig. 2). The discharge of potassium and carbon dioxide during this impregnation was also confirmed to enhance micropores and mesopores at high-temperature pyrolysis, as summarized in Table 1, where the PCBL-3 illustrated a type-IV curve characteristic with a slightly discernable loop hysteresis. This was quite different from the PCBL-P, due to showing a dominant microporosity characteristic of 757,455 m^2 g^{-1} at a total volume of 0.6177 cm^3 g^{-1}. For PCBL-3, KOH impregnation increased the porosity of the precursor to 992.360 m^2 g^{-1}, subsequently enhancing the possibility of the electrode having a high active site for the interaction of electrolytic ion charges, to produce an abundant electrical layer [38]. PCBL-5 also showed a type-IV curve with a more pronounced hysteresis loop than PCBL-3, indicating that the samples had a pore diameter expansion with mesopore size, as shown by their higher mean at 2.5 nm. Due to this pore characteristic, the sample provided a short ion transport pathway, causing the current to dramatically increase. These results consequently sacrificed their specific surface areas, as illustrated in Table 1.

At a high concentration in PCBL-7, the KOH impregnation showed a larger hysteresis loop than PCBL-5, suggesting that more intense wall reduction reactions produced larger pores [39]. This was in line with the SEM analysis shown in Fig. 2g–h, which indicated the reduction of their specific surface areas to a greater extent. However, this pore characteristic ensured that the electrode had reservoir properties for electrolyte ions. Based on Fig. 4, the complete pore size distribution of PCBLs ranged between 0.4 and 150 nm, showing the various micropores, mesopores and macropores. At high pyrolytic temperature treatment routes, the impregnation of KOH significantly led to a 3D hierarchical pore structure, with the chemical process relevantly increasing the microporosity in PCBL-3, PCBL-5, and PCBL-7. It also produced higher well-developed mesopores and macropores. This indicated that the impregnation adjusted the dominant size of the micropores and mesopores, from 1.8–1.2 nm and 5–3 nm, respectively. The combination of these three pores also increased the high performance of storage application, especially energy and power densities [40], whose mixture significantly affected the charge and discharge processes of the porous

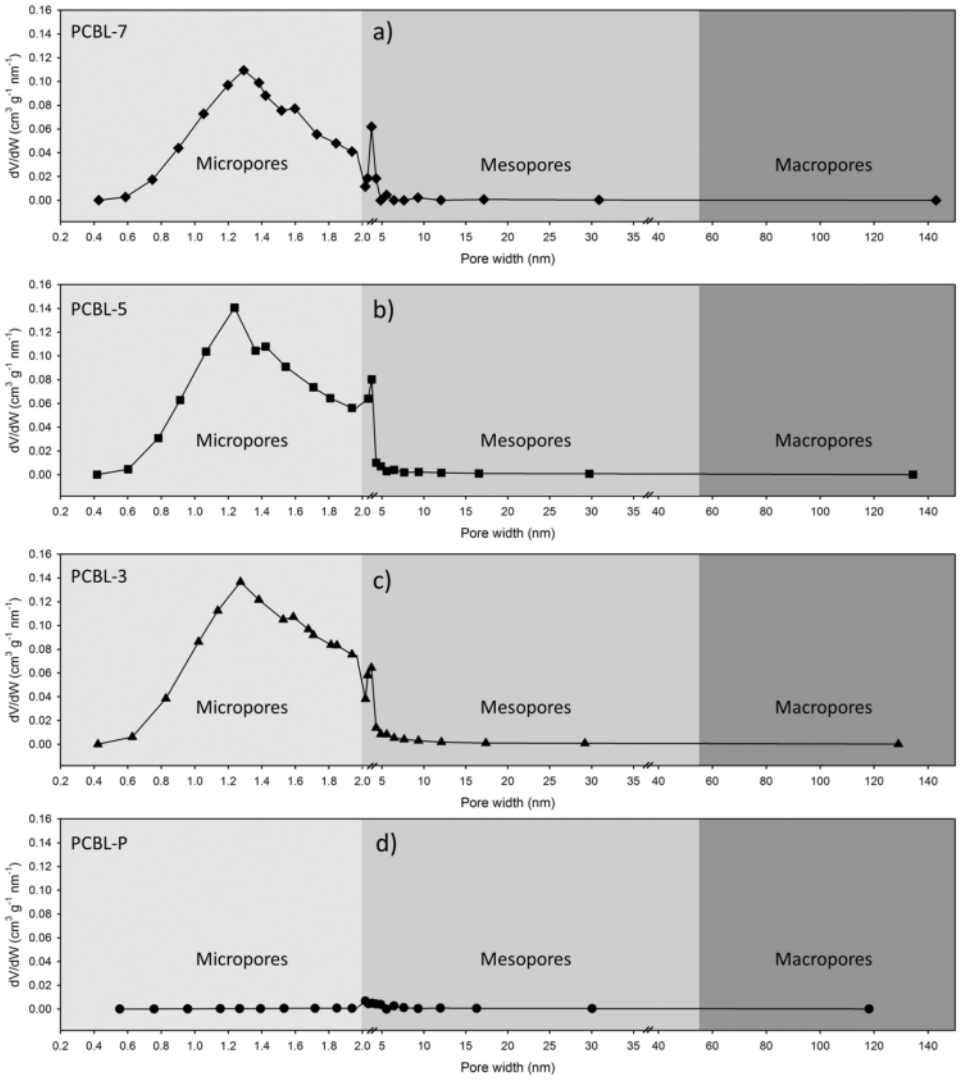

Fig. 4. Pore sizes distributions of PCBLs.

carbon-based supercapacitor.

Based on Fig. 4, the phase formation and microcrystal properties of the obtained PCBLs were reviewed on the XRD pattern. This indicated that the XRD pattern of the porous carbon showed the association of weak peaks with the (002) and (100) type reflection planes at 25° and 45°, subsequently characterizing its amorphous graphite phase [41,42]. The high interlayer spacing of the (002) diffraction around 0.35–0.39 nm (Table 2) also confirmed the low graphitization degree, due to the strong KOH impregnation effect on high-temperature pyrolysis [43]. At different concentrations of PCBL-3, PCBL-5, and PCBL-7, KOH impregnation shifted the diffraction peak (002) to a higher angle, indicating more defects in the disturbed carbon structure, leading to the initiation of rich hierarchical porosity [44]. This was in line with the SEM images and N_2 gas absorption/desorption profiles, which confirmed the 3D hierarchical pores structures. In addition, the diffraction peak (100) of PCBLs was found to be stronger, indicating a distorted carbon deposition structure [45]. In this study, the XRD pattern randomly showed weak sharp peaks at 36°, 39°, 47°, 48°, and 57°, indicating that small amounts of metal oxide compounds characterized potassium carbonate ($CaO/CaCO_3$) in small quantities [46]. This is agreement with EDS confirmation as shown in Table 3. This was a stratified treatment effect still abandoning the basic constituents of biomass [47]. Impurities of Ca, or Mg, and Si can inhibit the ion transport rate in the electrode material as well as cover the possibility of pore structure formation on the carbon surface [46]. However, the elemental oxygen attached to them as an oxide component can contribute to the electrochemical properties by increasing the wettability and self-heteroatomic properties of the pseudo-capacitance system [48]. This

Table 2
Interlayer spacing and lattice parameters of PCBLs.

PCBLs	$2\theta_{002}$ (°)	$2\theta_{100}$ (°)	d_{002} (nm)	d_{100} (nm)	L_c (nm)	L_a (nm)
PCBL-P	25.365	46.144	0.3508	0.1965	0.8579	1.6178
PCBL-3	23.441	44.919	0.3792	0.2016	0.5961	1.3353
PCBL-5	25.464	46.706	0.3495	0.1943	0.4106	0.8280
PCBL-7	24.760	45.441	0.3592	0.1994	0.5639	3.5608

Table 3
Elemental analysis of PCBLs.

PCBLs	Elementals					
	C (%)	O (%)	Mg (%)	Ca (%)	K (%)	Si (%)
PCBL-P	85.54	12.44	0.64	1.27	0.21	0.15
PCBL-3	87.22	10.61	0.71	1.35	0.03	0.08
PCBL-5	83.22	14.71	0.00	2.08	0.00	0.00
PCBL-7	86.28	11.63	0.60	1.19	0.22	0.07

analysis is strengthened through FTIR spectrum data, EDS data, and CV analysis. Table 2 summarized the interlayer spacing and microcrystalline dimensions of the (002) and (100) PCBLs diffraction. The spacing (002) was also relatively higher than the graphite structure, indicating a well-developed amorphous structure [49]. Furthermore, a relatively constant d_{100} characterized a weak graphite structure and was considered normal for organic waste-based carbon materials [50]. This indicated that the microcrystalline dimension of L_c was closely associated with the formation of an active site suitable for ion diffusion at the electrolyte/electrode interface [51]. The low L_c value also characterized multiple active sites in PCBLs, through their empirical equations. Therefore, PCBL-5 had high porosity properties initiating the formation of abundant electrical layers and their high charge conductivity. This was in line with the SEM analysis shown in Fig. 2e–f.

FTIR analysis provides information on the functional groups available on the PCBLs surface, with Fig. 5 showing the spectra of the porous activated carbon based on starfruit leaves of PCBL-P, PCBL-3, PCBL5, and PCBL-7. The results showed that vibrational bands were observed for OH/NH (3444 cm^{-1}), CH (2925 and 2854 cm^{-1}), C═O/C═N (1670 cm^{-1}) and CO/CN (1080 cm^{-1}) in the PCBLs spectrum. This indicated that the PCBLs-P exhibited relatively different spectra from the PCBL-3, PCBL-5, and PCBL-7 as precursors. It also showed that the PCBL-P had a relatively complex absorption band in the wavenumber of 4500–450 cm^{-1}. The OH/N—H strain mode of the hydroxy functional group was subsequently observed to be high at the peak of 3471 cm^{-1}, due to water being adsorbed and accompanied by the C═O stretching vibration at 1828 cm^{-1} [52]. In addition, the peak at 1557 cm^{-1} was determined for the C═C and O—H deformation vibrations in phenol and carboxylic acid [53]. This indicated that the appearance of the absorption band in the vicinity of 1000–900 cm^{-1} was ascribed to the C—O bonds in alcohols, phenols, and carboxylic acids [54]. At 718 cm^{-1}, the occurrence of the phenomenon was probably due to the presence of C—H, with the band at 524 cm^{-1} being assigned to C—O—H. After the routine stages of carbonization, as well as KOH and CO_2 activations, the intensity of these vibrational bands drastically decreased due to the partial elimination of nitrogen or oxygen functional groups, as shown in PCBL-3, PCBL-5, and PCBL-7 spectra. Although the range of this band did not shift dramatically, the broad strain bands of OH/N—H were still significantly reduced. This was due to the occurrence of water loss based on the KOH impregnated at high temperatures [55]. The peak around 1800–1700 cm^{-1} also surprisingly disappeared, characterizing the function of vaporized oxygen as CO and CO_2. From C═C and O—H, the vibrations of phenol and carboxylic acid were consequently confirmed in the 1555–1467 cm^{-1} band, although relatively low. In addition, the functional groups C—H and C—O—H were drastically reduced, indicating the optimum evaporation of volatile compounds, water content, and complex compounds due to the applied synthesis route. Besides that, some oxygen and nitrogen functions were still present in the obtained carbon contributing to the provision of wettability and hydrophilicity behaviors [56], which were in line with their elemental status (Table 3). According to Table 3, the elemental status of the PCBLs evaluated through the EDS technique was summarized, where carbon and oxygen status were high between 83–87% and 10–16%, respectively. This indicated that the carbon element dominating more than 3/4 of the PCBLs ensured the provision of high active sites on the electrode material, subsequently supporting the formation of an abundant electrical layer, as analyzed in the N_2 gas absorption profiles and SEM images (Figs. 2 and 3). The presence of elemental oxygen also justified the FTIR analysis contributing to the provision of self-doping heteroatoms, with the effects in-depthly analyzed through the CV and GCD profiles. In addition, other elements were observed in very small amounts of PCBLs, such as Mg, Ca, K and Si (Table 3), with their presence in the EDS spectrum increasing due to the selected synthesis route still retaining the basic and relatively low elemental constituents of the precursor.

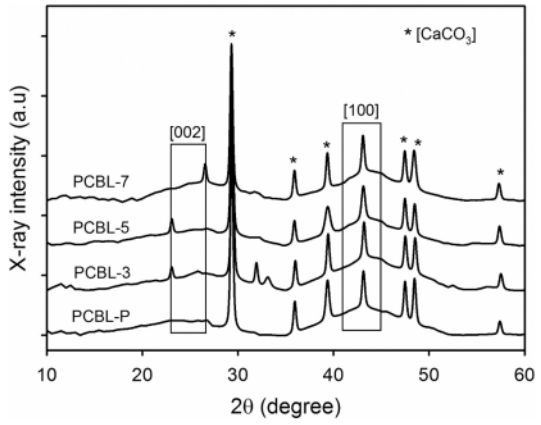

Fig. 5. X-ray diffraction patterns of PCBLs.

The electrochemical performance of the PCBLs electrodes was investigated through the CV, GCD, and EIS techniques, at a two-electrode configuration within a 1 M H_2SO_4 aqueous electrolyte. At different scanning rates, the CV profile was confirmed from 1 to 10 mV s^{-1} within the voltage window potentials between 0.0 and 1.0 V. The rectangular shape with pseudo-waves at a potential window of 0.4–0.6 V also reflected the combination of an electrical double layer and a pseudo-capacitance charge-storage mechanism, using binder-free PCBLs as the working electrode power-source. These data indicated that the two-electrode configuration of PCBLs exhibited a specific capacitance of 83–285 F g^{-1} at 1 mV s^{-1}, confirming that KOH impregnation on high-temperature pyrolysis obtained different capacities and reversibility regarding the distinguished concentrated solutions [57]. Furthermore, KOH impregnation drastically increased specific capacitance from 43 to 166 F g^{-1}, as shown by PCBL-P and PCBL-3. The addition of 0.3–0.5 m/L also provided an increase of 166–285 F g^{-1} in a peak specific capacitance of 71.68%, due to the presence of abundant micropores and higher reactive site interface (Table 3) [58]. The pseudo-wave peaks subsequently widened to a potential window of 0.2–0.6 V, indicating an increase of self-oxygen doping to the electrode capacitive increase (Table 3) [48]. This indicated that increasing the KOH concentration in PCBL-7 was found to decrease the current density of approximately 43.6%, leading to the specific capacitance being reduced from 285 to 199 F g^{-1}. It also showed that the degraded active site due to the widening of the pores in PCBL-7 led to less storage space in the electrode, where lower oxygen reduced pseudo-behaviors. In addition, the diffusion-reaction of the electrode-electrolyte interface on KOH-impregnated PCBLs was examined through different scanning rates between 1 and 5 mV s^{-1}, as shown in Fig. 6b–d. When the scan rate increased from 1 to 5 mV s^{-1}, the limiting current density elevated with the curve profile maintaining a wide distorted rectangular shape, indicating normal EDLC properties. This hypothesized that the gradient of the electrolyte ion transfusion changed during the forward and backward scans [59]. The results also showed the effect of electrolytic ion diffusion around the surface of PCBLs with increasing scanning rate. Based on this study, the dependence of the current density on the scanning rate provided insights into the mechanism of charge storage through electrochemical capacitors. At the scanning rates between 1 and

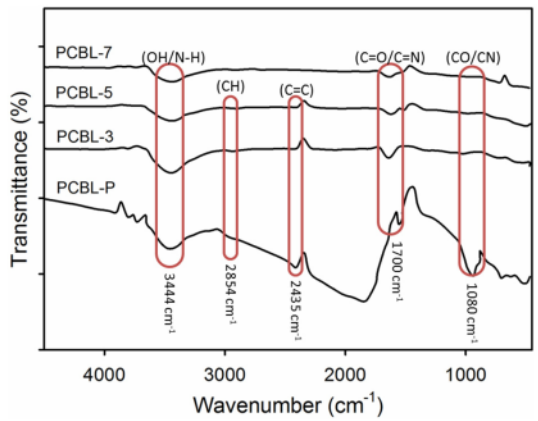

Fig. 6. IR spectrums of PCBLs.

10 mV s^{-1}, the diffusion-controlled specific capacitance ratio of the PCBLs electrode is shown in Fig. 7e, where the capacitive contribution decreased as the evaluation value increased. When this rate was relatively low, the electrolyte ions had sufficient time to enter the space within the electrode. This indicated that the increase in the high scanning rate caused the inability of the electrolyte ions to completely access the interior of the active material at high current densities, although only the outer surface of the electrode was used for charge storage [60]. The relatively weak mesoporous structure was also insufficient to provide adequate access for additional ionic storage.

Galvanostatic charge/discharge (GCD) was implemented as an in-depth approach to evaluate the capacitive properties, as well as the energy and power densities of PCBLs electrodes (Fig. 7f–h). This showed that the GCD profile indicated an isosceles triangle shape with CV-like trend of variation in specific capacitance, from 39 to 293 F g^{-1} at a current density and scan rate of 1 A g^{-1} and 1 mV s^{-1}, respectively. In the charging process, the GCD profile was in line with a waveform shape (Fig. 7f), indicating ion degradation due to oxygen self-doping as a Faradaic storage behavior [23]. The observed "IR drop" quite confirmed the resistance of the PCBLs at 0.213, 0.172, 0.111, and 0.097 Ω. These lower values indicated a higher conductivity from the PCBL-P to PCBL-7 electrodes, with the KOH-activating agent significantly increasing the conductivity of the precursor at approximately 54.46%. Moreover, the obtained specific capacitance drastically increased from 39 to 293 F g^{-1}, as shown in PCBL-P to PCBL-5, where the KOH-activating agent was able to dramatically increase the specific surface area of the precursor from 35 to 992.360 m^2 g^{-1}. This led to the formation of abundant electroactive layers, initiating excellent capacitive properties. At 0.5 mol/L, KOH impregnation treatment provided a well dispersed and rooted porosity structure on the electrode surface, leading to an increase in the interconnected pores and reactive sites [61]. However, increasing the KOH concentration to 0.7 mol/L led to a consequent reduction in surface area, widening the pore size and decreasing their capacitive properties by 26.66% to 215 F g^{-1}. The columbic efficiency of the PCBLs electrodes was also interpreted through the ratio between the charge and

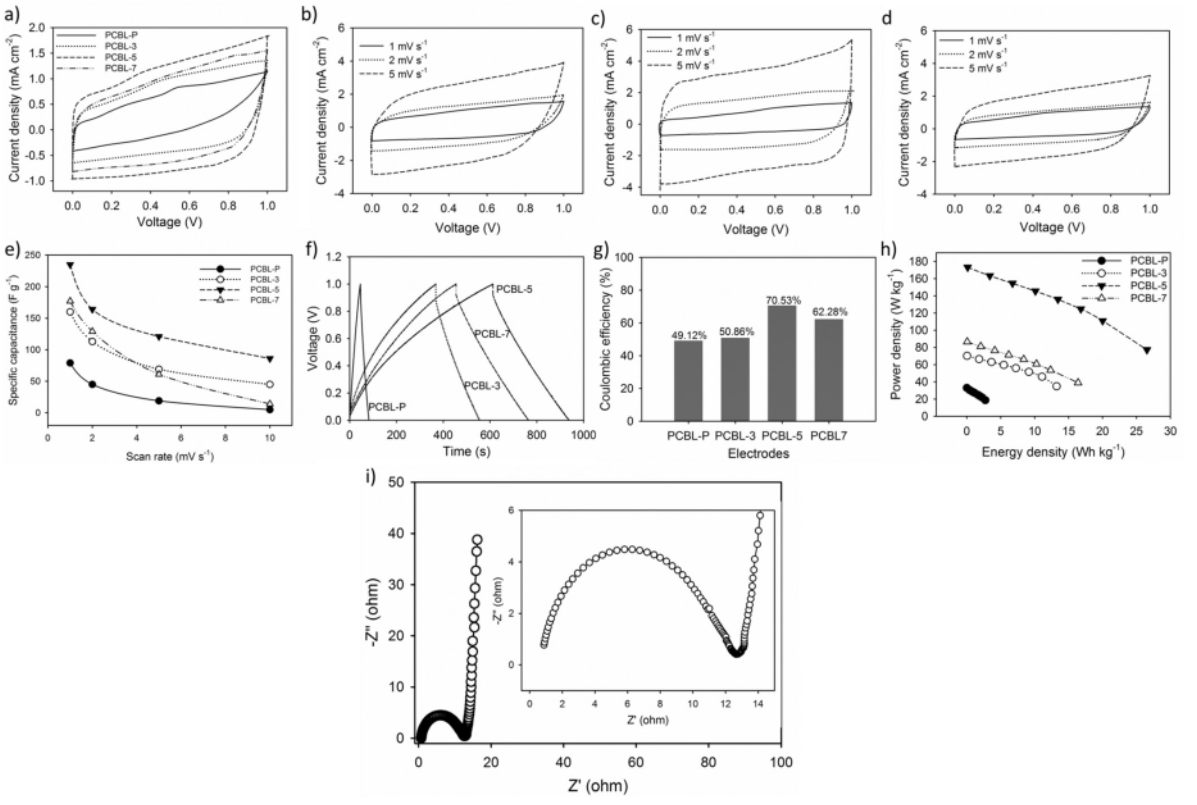

Fig. 7. Electrochemical performance in 1 M H_2SO_4 for (a) CV profile of PCBLs at 1 mV s^{-1}, (b) CV profile of PCBL-3 at 1, 2, and 5 mV s^{-1}, (c) CV profile of PCBL-5 at 1, 2, and 5 mV s^{-1}, (d) CV profile of PCBL-3 at 1, 2, and 5 mV s^{-1}, (e) specific capacitance at different scan rate, (f) GCD profile of PCBLs at 1 A g^{-1}, (g) coulombic efficiency of PCBLs at 1 A g^{-1}, (h) Ragone plot of PCBLs, and (i) Nyquist plots of PCBL-5 electrode.

discharging times on the GCD profile, as illustrated in Fig. 7g. This indicated that the efficiency obtained for PCBL-P, PCBL-3, PCBL-5, and PCBL-7 was 49.12, 50.85, 70.53, and 62.28%, respectively. An increase in this efficiency was also found with increased KOH impregnation, confirming the high collective interpenetration and accessibility of the electrolytes [62]. In addition, the energy density of the symmetric electr-based PCBLs was obtained between 2 and 26 Wh kg^{-1} at a high power density of 32–173 W kg^{-1}, as shown on the Ragone plot (Fig. 7h). This showed that the PCBL-5 electrode provided a significant increase in the energy density (94%) of 26.5439 Wh kg^{-1}, at a high power density of 173.45 W kg^{-1}, indicating a higher result than most previous reports on biomass-based supercapacitors. At a concentration of 0.5 mol/L, KOH impregnation treatment on starfruit leaf precursors allowed the formation of a micro-mesoporosity optimized for activated carbon. The modification of the hierarchically-connected pore structure also facilitated the intercalation between the different crystallographic structures, which significantly increased the cyclical stability, as well as the combined energy and power densities [63]. During th cycle, the obtained supercapacitors subsequently exhibited the reversibility of charge and discharge profiles over the full operating voltage range with relatively low energy losses, compared to metal oxide electrodes. This performance indicated that the PCBL-5 electrodes designed in a binder-free dual configuration had very high capacitance capabilities than the reported results [64,65].

The EIS (electrochemical impedance) spectrum of the PCBL-5 electrode was further investigated in Fig. 7i, to observe its high electrochemical properties. This showed that the Nyquist plot of the PCBL-5 sample was divided into two parts based on a semicircle and a diagonal-vertical line in the high and low-frequency regions, respectively. In the high region, the Nyquist plot intercepting with the real axes and semicircular diameter is closely related to fast ionic responses in a 3D hierarchical porous structure and low contact resistance [66]. Furthermore, PCBL-5 showed a steep slope in the low region, confirming its fast ionic diffusion and migration ability.

To show reliable electrochemical properties, the performances of the PCBL-3, PCBL-5, and PCBL-7 electrodes were reviewed through different aqueous electrolytes, including 1 M NaOH and Na_2SO_4, respectively. The CV profiles are illustrated in Fig. 8a and b, where a non-ideal rectangular shape was observed, accompanied by a waveform along the potential window. This confirmed the normal EDLC properties embellished by the pseudo-capacitance effect [67]. As previously shown, the oxidative functional groups of carbonaceous materials underwent the faradic redox reactions caused by the interactions involving the electrolyte ion and the bound FG (functional groups) [68]. This indicated that the NaOH electrolyte was advantageous for the function/doping of carbon materials, to subsequently increase pseudo-capacitance than Na_2SO_4. In the carbon material, the presence of oxygen functional groups increased the apparent capacitance contribution in the aqueous electrolyte, which led to the elevation of the overall capacitive reactance of the electrode. Moreover, the maximum capacitance found at the PCBL-5 electrode was 189 and 175 F g^{-1} in the NaOH and Na_2SO_4 electrolytes, respectively. These were in line with the data on the H_2SO_4 electrolyte, although the values were lower. This was subsequently due to the high electrolyte conductivity of H_2SO_4, compared to NaOH and Na_2SO_4. The five times larger radius of the hydrated Na^+ ion also limited high performances [69].

At 1 to 10 mV s^{-1}, the specific capacitance-controlled diffusion of NaOH and Na_2SO_4 in the PCBL-3, PCBL-5, and PCBL-7 electrodes are shown in Fig. 8c and d, where the capacitive contribution subsequently reduced as the scanning rate increased. When this rate became relatively low, the electrolyte ions had sufficient time to enter the space within the electrode. This indicated that a higher scanning rate caused the inability of the ions to completely access the interior of the active material at increased current densities, although only the outer surface of the electrode was used for charge storage [45]. The relatively weak mesoporous structure was also insufficient in providing adequate access for additional ionic storage. This led to a considerable capacitive reduction of 64% in the NaOH electrolyte, as shown at the PCBL-5 electrode. Moreover, Na_2SO_4 interestingly maintained 76% higher capacitive properties than the NaOH electrolytes in 10 mV s^{-1}, although the specific capacitance value was relatively low. This was closely related to the contribution of Na^+ and SO_4^{2-} ions, which effectively assessed the mesopores within the PCBLs [70]. Based on CV analysis, the capacitive properties of PCBLs was observed in stages from large to small, through the electrolyte differences at H_2SO_4 > NaOH > Na_2SO_4. The PCBL-3, PCBL-5, and PCBL-7 electrodes were also confirmed by Galvanostatic charge/discharge in different aqueous electrolytes of 1 M NaOH and Na_2SO_4, as shown in Fig. 8e and f. Subsequently, the GCD profile indicated a non-ideal isosceles triangle curved form with confirmed electrolyte ion degradation, where the contribution of the oxidative functional groups underwent a redox reaction. This indicated that the ionic charge was degraded during the charging process, initiating the apparent PCBLs capacitance. In this condition, the reaction also led to the columbic efficiency being highly degraded compared to the H_2SO_4

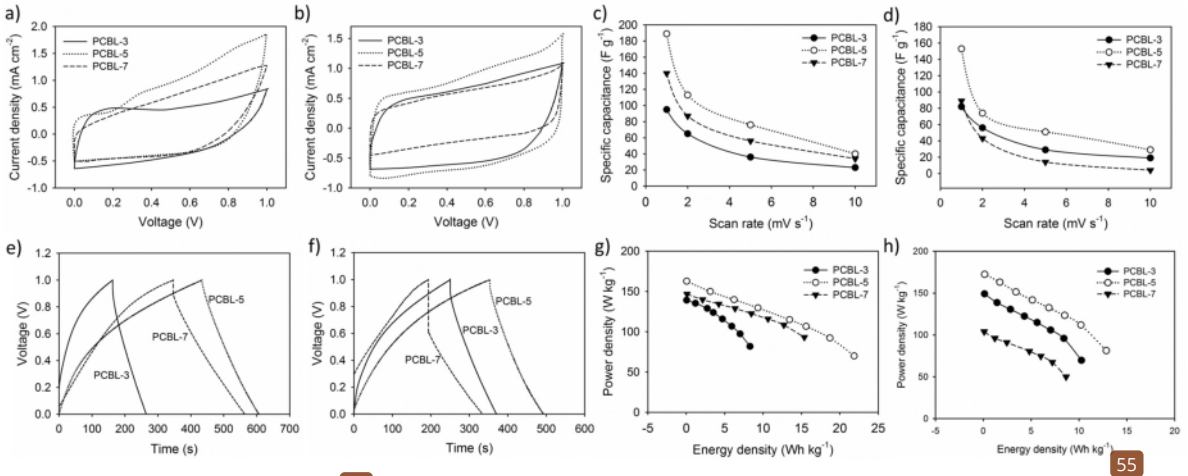

Fig. 8. Electrochemical performance for (a) CV file of PCBLs in 1 M NaOH, (b) CV profile of PCBLs in 1 M Na_2SO_4, (c) specific capacitance at different scan rate in 1 M NaOH, (d) specific capacitance at different scan rate in 1 M Na_2SO_4, (e) GCD profile of PCBLs in 1 M NaOH, (f) GCD profile of PCBLs in 1 M Na_2SO_4, (g) Ragone plot of PCBLs in 1 M NaOH, (h) Ragone plot of PCBLs in 1 M Na_2SO_4.

electrolyte. For NaOH and Na_2SO_4, these efficiencies were observed at 61.56, 46.59, and 53.51% for PCBL-3, PCBL-5, and PCBL-7, respectively. In this study, the self-doping heteroatoms of 10–14% significantly elicited a pseudo-capacitance effect, which was confirmed in NaOH, accompanied by Na_2SO_4 and H_2SO_4. This indicated that the overall capacitance of PCBLs was maximally increased. In aqueous NaOH electrolytes, the PCBL-3, PCBL-5, and PCBL-7 electrodes showed specific capacitances of 111, 197, and 168 F g^{-1} at a current density and scan rate of 1 A g^{-1} and 1 mV s^{-1}, respectively. This was in line with the data shown for the H_2SO_4 electrolytes, although the capacitive reduction was nearly 50% due to ionic mobility and low conductivity. On the other hand, the Na_2SO_4 electrolyte showed different trends with specific capacitance values of 145, 187, and 92 F g^{-1} for PCBL-3, PCBL-5, and PCBL-7, respectively. For the PCBL-7 electrode, the least capacitive properties were observed and accompanied by a large "IR drop", indicating the incompatibility of the Na_2SO_4 electrolyte to the pore size distribution development. In addition, the reduced surface area accompanied by a relatively narrow mean pore impeded the ionic diffusion pathway, leading to low capacitive properties and high resistance [71].

Overall, different aqueous electrolytes generally exhibited various capacitive properties, due to the contribution of the charges to the properties. This was because of the ionic mobility, hydration radius, and conductivity of the electrolyte on charge/ion exchange and diffusion [72]. It also showed that a smaller H^+ dehydration radius sphere allowed the cation charge to have the greatest conductivity, therefore, initiating the fast transfer and high ion adsorption at the electrolyte/electrode interface [70,73]. The SO_4^{2-} anion also showed a larger hydration radius sphere than the OH^-, leading to the reduction of the ions having the ability to form an electric double-layer [74]. This plausible explanation indicated that the H_2SO_4 electrolyte had the highest capacitive properties of PCBLs, accompanied by NaOH and Na_2SO_4.

The energy and power densities of PCBL-3, PCBL-5, and PCBL-7 were also evaluated in aqueous electrolytes (NaOH and H_2SO_4), through the Ragone plots illustrated in Fig. 8g and h. In NaOH electrolyte, the energy densities obtained from the electrodes PCBL-3, PCBL-5, and PCBL-7 were 8.29, 21.85, and 15.37 Wh kg^{-1} at power densities of 139.19, 162.78, and 146.72 W kg^{-1}, respectively. Furthermore, the Na_2SO_4 electrolyte displayed energy densities of 11.78, 16.12, and 8.01 Wh kg^{-1} for PCBL-3, PCBL-5, and PCBL-7 at power densities of 163.47, 178.44 and 124.34 W kg^{-1}, respectively. This result was relatively lower than that of the H_2SO_4 electrolyte (Fig. 7h). However, the specific capacitance and energy density generated in this study was competitive with other studies, especially in the novelty provision, such as efficiency of the electrode material designed as solid consolidated carbon coin binder-free which optimized low internal resistance and high conductivity, two-electrode configuration system analysis, self-oxygen doped, and 3D pore hierarchical properties combination [24,75]. These were based on the *Averrhoa bilimbi* leaves biomass waste, as shown in Table 4.

4. Conclusion

Herein, a biomass-related hierarchical porous carbon with self-oxygen doped was obtained from *Averrhoa bilimbi* leaves through a facile, simple, cheap, and sustainable approach, using a one-way KOH impregnation at high-temperature pyrolysis. In this analysis, the precursor was converted into a binder-free electrode design, using combined methods of pre-carbonization, chemical impregnation, carbonization, and physical activation. This indicated that PCBLs material exhibited high porosity with specific surface area and abundant micropores of 1000 m^2 g^{-1} and 78.66%, as well as adjustable mesopores, respectively. The porosity and oxygen functional group were also controlled by the KOH-impregnated solution, where PCBL-5 material performed high micropores with doped self-oxygen of 14.71%. This indicated their high electrochemical performances in different aqueous electrolytes. For symmetric supercapacitor, PCBL-5 electrode had high specific capacitances of 293, 197, and 178 F g^{-1} in aqueous 1 M H_2SO_4, NaOH, and Na_2SO_4, respectively. It also exhibited a columbic efficiency of 70.53% at a current density of 1.0 A g^{-1}. Therefore, a new approach was developed to obtain hierarchically-interconnected porous carbon material with enriched self-oxygen doped, for a high-quality supercapacitor electrode.

Table 4
Electrochemical of porous carbon biomass-based for supercapacitor electrodes.

Sources	Electrolyte	Electrode type	C_{sp} (F g^{-1})	E (Wh kg^{-1})	P (W kg^{-1})	Ref
Jujube fruits	6 M KOH	Two-electrode	145.6	22.7	368	[19]
Jujube fruits	1 M Et4NBF4/AN	Two-electrode	54.7	23.7	629	[19]
Watermelon	1 M H_2SO_4	Two-electrode	226	25.4	180	[20]
Watermelon	6 M KOH	Two-electrode	171	19.1	180	[20]
Averrhoa bilimbi leaf	1 M Na_2SO_4	Two-electrode	149	10.50	116.35	[27]
Feather finger grass flower	6 M KOH	Two-electrode	120	18.75	370	[75]
PCBL-5	1 M H_2SO_4	Two-electrode	293	26.54	178.44	This work

CRediT authorship contribution statement

Erman Taer: Conceptualization, Methodology, **Apriwandi**: Formal analysis, Data curation, Writing - Original draft preparation, Writing - Reviewing & Editing, **Nursyafni**: Resources, **Rika Taslim**: Visualization, Validation.

Declaration of competing interest

The authors declare that they have no known competing financial interests or personal relationships that could have appeared to influence the work reported in this paper.

Acknowledgements

The research was financially supported by second years Project of Word Class Research (WCR) in *Kementerian Pendidikan, Kebudayaan, Riset, dan Teknologi*, Republic of Indonesia with the title "High energy and power densities of supercapacitor for the optimization of electrode supply process".

References

[1] A. González, E. Goikolea, J.A. Barrena, R. Mysyk, Review on supercapacitors: technologies and materials, Renew. Sust. Energ. Rev. 58 (2016) 1189–1206, https://doi.org/10.1016/j.rser.2015.12.249.

[2] E.E. Miller, Y. Hua, F.H. Tezel, Materials for energy storage: review of electrode materials and methods of increasing capacitance for supercapacitors, J. Energy Storage 20 (2018) 30–40, https://doi.org/10.1016/j.est.2018.08.009.

[3] Z. Li, D. Guo, Y. Liu, H. Wang, L. Wang, Recent advances and challenges in biomass-derived porous carbon nanomaterials for supercapacitors, Chem. Eng. J. (2020), 125418, https://doi.org/10.1016/j.cej.2020.125418.

[4] X. Li, J. Zhang, B. Liu, Z. Su, A critical review on the application and recent developments of post-modified biochar in supercapacitors, J. Clean. Prod. 310 (2021), 127428, https://doi.org/10.1016/j.jclepro.2021.127428.

[5] X. Liu, C. Ma, J. Li, B. Zielinska, R.J. Kalenczuk, X. Chen, P.K. Chu, T. Tang, E. Mijowska, Biomass-derived robust three-dimensional porous carbon for high volumetric performance supercapacitors, J. Power Sources 413 (2019) 1–9, https://doi.org/10.1016/j.jpowsour.2018.11.032.

[6] L. Zhang, D. Huang, N. Hu, C. Yang, M. Li, H. Wei, Z. Yang, Y. Su, Y. Zhang, Three-dimensional structures of graphene/polyaniline hybrid films constructed by steam activation of water for high-performance supercapacitors, J. Power Sources 342 (2017) 1–8, https://doi.org/10.1016/j.jpowsour.2016.11.068.

[7] A. Gopalakrishnan, S. Badhulika, Effect of self-doped heteroatoms on the performance of biomass-derived carbon for supercapacitor applications, J. Power Sources 480 (2020), 228830, https://doi.org/10.1016/j.jpowsour.2020.228830.

[8] J. Wang, F. Zheng, Y. Yu, P. Hu, M. Li, J. Wang, J. Fu, Q. Zhen, S. Bashir, J.L. Liu, Symmetric supercapacitors composed of ternary metal oxides (NiO/V2O5/MnO2) nanoribbon electrodes with high energy storage performance, Chem. Eng. J. 426 (2021), https://doi.org/10.1016/j.cej.2021.131804.

[9] D. Chu, F. Li, X. Song, H. Ma, L. Tan, H. Pang, X. Wang, D. Guo, B. Xiao, A novel dual-tasking flower cube NiFe2O4-NiCo-LDH@rGO hierarchical material for high preformance supercapacitor and glucose sensor, J. Colloid Interface Sci. 568 (2020) 130–138, https://doi.org/10.1016/j.jcis.2020.02.012.

[10] Z. Lu, J. Foroughi, C. Wang, H. Long, G.G. Wallace, Superelastic hybrid CNT/graphene fibers for wearable energy storage, Adv. Energy Mater. 8 (2018) 1–10, https://doi.org/10.1002/aenm.201702047.

[11] S. Zhang, W. Xia, Q. Yang, Y. Valentino Kaneti, X. Xu, S.M. Alshehri, T. Ahamad, M. S.A. Hossain, J. Na, J. Tang, Y. Yamauchi, Core-shell motif construction: highly graphitic nitrogen-doped porous carbon electrocatalysts using MOF-derived carbon@COF heterostructures as sacrificial templates, Chem. Eng. J. 396 (2020), 125154, https://doi.org/10.1016/j.cej.2020.125154.

[12] Z. Liu, J. Hu, F. Shen, D. Tian, M. Huang, J. Fu, Z. Zou, L. Zhao, Y. Zeng, Trichoderma bridges waste biomass and ultra-high specific surface area carbon to achieve a high-performance supercapacitor, J. Power Sources 497 (2021), 229880, https://doi.org/10.1016/j.jpowsour.2021.229880.

[13] A. Xie, J. Dai, Y. Chen, N. Liu, W. Ge, P. Ma, R. Zhang, Z. Zhou, S. Tian, C. Li, Y. Yan, NaCl-template assisted preparation of porous carbon nanosheets started from lignin for efficient removal of tetracycline, Adv. Powder Technol. 30 (2019) 170–179, https://doi.org/10.1016/j.apt.2018.10.020.

[14] G. Jiang, R.A. Senthil, Y. Sun, T.R. Kumar, J. Pan, Recent progress on porous carbon and its derivatives from plants as advanced electrode materials for supercapacitors, J. Power Sources 520 (1) (2022), 230886, https://doi.org/10.1016/j.jpowsour.2021.230886.

[15] O. Boujibar, F. Ghamouss, A. Ghosh, O. Achak, T. Chafik, Efficient CO2 capture by ultra-high microporous activated carbon made from natural coal, Chem. Eng. Technol. 44 (2021) 148–155, https://doi.org/10.1002/ceat.202000138.

[16] Z. Guo, X. Kong, X. Wu, W. Xing, J. Zhou, Y. Zhao, S. Zhuo, Heteroatom-doped hierarchical porous carbon via molten-salt method for supercapacitors, Electrochim. Acta 360 (2020), 137022, https://doi.org/10.1016/j.electacta.2020.137022.

[17] H. Peng, S. Qi, Q. Miao, R. Zhao, Y. Xu, G. Ma, Z. Lei, Formation of nitrogen-doped holey carbon nanosheets via self-generated template assisted carbonization of polyimide nanoflowers for supercapacitor, J. Power Sources 482 (2021), 228993, https://doi.org/10.1016/j.jpowsour.2020.228993.

[18] S. Majid, A.S.G. Ali, W.Q. Cao, R. Reza, Q. Ge, Biomass-derived porous carbons as supercapacitor electrodes-a review, New Carbon Mater. 36 (2021) 546–572, https://doi.org/10.1016/S1872-5805(21)60038-0.

[19] V. Yang, R.A. Senthil, J. Pan, T.R. Kumar, Y. Sun, X. Liu, Hierarchical porous carbon derived from jujube fruits as sustainable and ultrahigh capacitance material for advanced supercapacitors, J. Colloid Interface Sci. 579 (2020) 347–356, https://doi.org/10.1016/j.jcis.2020.06.080.

[20] P. Zhang, J. Mu, Z. Guo, S.I. Wong, J. Sunarso, Y. Zhao, W. Xing, J. Zhou, S. Zhuo, Watermelon Peel-derived heteroatom-doped hierarchical porous carbon as a high-performance electrode material for supercapacitors, ChemElectroChem. 8 (2021) 1196–1203, https://doi.org/10.1002/celc.202100267.

[21] Y. Zhang, R. Zhao, Y. Li, X. Zhu, B. Zhang, X. Lang, L. Zhao, B. Jin, Y. Zhu, Q. Jiang, Potassium-ion batteries with novel N, O enriched corn silk-derived carbon as anode exhibiting excellent rate performance, J. Power Sources 481 (2021), 228644, https://doi.org/10.1016/j.jpowsour.2020.228644.

[22] K. Aruchamy, K. Dharmalingam, C.W. Lee, D. Mondal, N. Sanna Kotrappanavar, Creating ultrahigh surface area functional carbon from biomass for high performance supercapacitors and facile removal of emerging pollutants, Chem. Eng. J. 427 (2022), 131477, https://doi.org/10.1016/j.cej.2021.131477.

[23] L.H. Zheng, M.H. Chen, S.X. Liang, Q.F. Lü, Oxygen-rich hierarchical porous carbon derived from biomass waste-kapok flower for supercapacitor electrode, Diam. Relat. Mater. 113 (2021), 108267, https://doi.org/10.1016/j.diamond.2021.108267.

[24] Y. Zhang, C. Wu, S. Dai, L. Liu, H. Zhang, W. Shen, W. Sun, C.Ming Li, Rationally tuning ratio of micro- to meso-pores of biomass-derived ultrathin carbon sheets toward supercapacitors with high energy and high power density, J. Colloid Interface Sci. 606 (2022) 817–825, https://doi.org/10.1016/j.jcis.2021.08.042.

[25] X. Xu, L. Yang, K. Zhuo, Z. Zhang, Q. Du, C. Wang, Y. Chen, Y. Zhao, Honeysuckle flowers-derived hierarchical porous carbon matching with ionic liquid electrolyte for high-energy supercapacitors, J. Energy Storage. 41 (2021), 102988, https://doi.org/10.1016/j.est.2021.102988.

[26] Sub-directorate of Horticulture Statistics, Statistics of Anual Fruit and Vegetable Plants, 2019.

[27] E. Taer, Apriwandi, Rosyafni, R. Taslim, High potential of Averrhoa bilimbi leaf waste as porous activated carbon source for sustainable electrode material supercapacitor, in, J. Phys. Conf. Ser. (2021), 012051, https://doi.org/10.1088/1742-6596/2049/1/012051.

[28] N.N. Mohameda, L.S. Yuan, L.S. Ling, H.C. Siong, S. Chandren, H. Nur, Preparation of hierarchical porous carbon derived from Averrhoa bilimbi and its diffusion properties, J. Teknol. (Sciences Eng. 69 (2014) 61–64, https://doi.org/10.11113/jt.v69.3206.

[29] E. Taer, R. Taslim, Brief review: preparation techniques of biomass based activated carbon monolith electrode for supercapacitor applications, in: AIP Conf. Proc, 2018, https://doi.org/10.1063/1.5021192, pp. 020004-1-020004–4.

[30] E. Taer, K. Natalia, A. Apriwandi, R. Taslim, A. Agustino, R. Farma, The synthesis of activated carbon nano fiber electrode made from acacia leaves (Acacia mangium wild) as supercapacitors, Adv. Nat. Sci. Nanosci. Nanotechnol. 11 (2020) 25007, https://doi.org/10.1088/2043-6254/ab8b60.

[31] E. Taer, L. Pratiwi, W.S. Apriwandi, R.Taslim Mustika, Agustino, Three-dimensional pore structure of activated carbon monolithic derived from hierarchically bamboo stem for supercapacitor application, Commun. Sci. Technol. 5 (2020) 22–30, https://doi.org/10.21924/cst.5.1.2020.180.

[32] E. Taer, Y. Susanti, A. Awitdrus, S. Sugianto, R. Taslim, R.N. Setiadi, S. Bahri, A. Agustino, P. Dewi, B. Kurniasih, The effect of CO2 activation temperature on the physical and electrochemical properties of activated carbon monolith from banana stem waste, AIP Conf. Proc. 1927 (2018), https://doi.org/10.1063/1.5021209, 030016–1–030016–.

[33] P. González-García, Activated carbon from lignocellulosics precursors: a review of the synthesis methods, characterization techniques and applications, Renew. Sust. Energ. Rev. 82 (2018) 1393–1414, https://doi.org/10.1016/j.rser.2017.04.117.

[34] R. Ma, S. Ding, H. Ren, Y. Liu, Sakura-based activated carbon preparation and its performance in supercapacitor applications, RSC Adv. 9 (2019) 2474–2483, https://doi.org/10.1039/c8ra09685f.

[35] H. Liu, F. Gao, Q. Fan, C. Wei, C. Ma, J. Shi, Preparation of novel 3D hierarchical porous carbon membrane as flexible free-standing electrode for supercapacitors, J. Electroanal. Chem. 873 (2020), 114409, https://doi.org/10.1016/j.jelechem.2020.114409.

[36] Q. Zhang, K. Han, S. Li, M. Li, J. Li, K. Ren, Synthesis of garlic skin-derived 3D hierarchical porous carbon for high-performance supercapacitors, Nanoscale 10 (2018) 2427–2437, https://doi.org/10.1039/c7nr07158b.

[37] X.L. Dong, A.H. Lu, B. He, W.C. Li, Highly microporous carbons derived from a complex of glutamic acid and zinc chloride for use in supercapacitors, J. Power Sources 327 (2016) 535–542, https://doi.org/10.1016/j.jpowsour.2016.07.100.

[38] G.A. Yakaboylu, C. Jiang, T. Yumak, J.W. Zondlo, J. Wang, E.M. Sabolsky, Engineered hierarchical porous carbons for supercapacitor applications through chemical pretreatment and activation of biomass precursors, Renew. Energy 163 (2021) 276–287, https://doi.org/10.1016/j.renene.2020.08.092.

[39] R.T. Ayinla, J.O. Dennis, H.M. Zaid, Y.K. Sanusi, F. Usman, L.L. Adebayo, A review of technical advances of recent palm bio-waste conversion to activated carbon for energy storage, J. Clean. Prod. 229 (2019) 1427–1442, https://doi.org/10.1016/j.jclepro.2019.04.116.

[40] E. Taer, A. Apriwandi, A. Agustino, M.R. Dewi, R. Taslim, Porous hollow biomass-based carbon nanofiber/nanosheet for high-performance supercapacitor, Int. J. Energy Res. 46 (2022) 1467–1480, https://doi.org/10.1002/er.7262.

[41] J. Sodtipinta, C. Ieosakulrat, N. Poonyapat, P. Kidkhunthod, N. Chanlek, T. Amornsakchai, P. Pakawatpanurut, Interconnected open-channel carbon nanosheets derived from pineapple leaf fiber as a sustainable active material for supercapacitors, Ind. Crop. Prod. 104 (2017) 13–20, https://doi.org/10.1016/j.indcrop.2017.04.015.

[42] V. Barranco, M.A. Lillo-Rodenas, A. Linares-Solano, A. Oya, F. Pico, J. Ibañez, F. Agullo-Rueda, J.M. Amarilla, J.M. Rojo, Amorphous carbon nanofibers and their activated carbon nanofibers as supercapacitor electrodes, J. Phys. Chem. C 114 (2010) 10302–10307, https://doi.org/10.1021/jp1021278.

[43] Y. Xi, D. Yang, X. Qiu, H. Wang, J. Huang, Q. Li, Renewable lignin-based carbon with a remarkable electrochemical performance from potassium compound activation, Ind. Crop. Prod. 124 (2018) 747–754, https://doi.org/10.1016/j.indcrop.2018.08.018.

[44] E. Taer, A. Apriwandi, R. Taslim, A. Agutino, D.A. Yusra, Conversion syzygium polyanthum leaves biomass waste to porous activated carbon nanosheet for boosting supercapacitor performances, J. Mater. Res. Technol. 9 (2020) 13332–13340, https://doi.org/10.1016/j.jmrt.2020.09.049.

[45] A. Apriwandi, E. Taer, R. Farma, R.N. Setiadi, E. Amiruddin, A facile approach of micro-mesopores structure binder-free coin/monolith solid design activated carbon for electrode supercapacitor, J. Energy Storage. 40 (2021), 102823, https://doi.org/10.1016/j.est.2021.102823.

[46] E. Taer, B.K.L. Apriwandi, R.Taslim Dalimunthe, A rod-like mesoporous carbon derived from agro-industrial cassava petiole waste for supercapacitor application, J. Chem. Technol. Biotechnol. 96 (2021), https://doi.org/10.1002/jctb.6579.

[47] S. Saini, P. Chand, A. Joshi, Biomass derived carbon for supercapacitor applications: review, J. Energy Storage. 39 (2021), 102646, https://doi.org/10.1016/j.est.2021.102646.

[48] E. Taer, R. Taslim, A. Apriwandi, Ultrahigh capacitive supercapacitor derived from self-oxygen doped biomass-based 3D porous carbon sources, ChemNanoMat. 8 (2022), e202100388, https://doi.org/10.1002/cnma.202100388.

[49] F. Márquez-Montesino, N. Torres-Figueredo, A. Lemus-Santana, F. Trejo, Activated carbon by potassium carbonate activation from pine sawdust (Pinus montezumae Lamb.), Chem. Eng. Technol. 43 (2020) 1716–1725, https://doi.org/10.1002/ceat.202000051.

[50] A.M. Abioye, F.N. Ani, Recent development in the production of activated carbon electrodes from agricultural waste biomass for supercapacitors: a review, Renew. Sust. Energ. Rev. 52 (2015) 1282–1293, https://doi.org/10.1016/j.rser.2015.07.129.

[51] M. Deraman, R. Daik, S. Soltaninejad, N.S.M. Nor, R. Awitdrus, N.F. Farma, N. H. Mamat, M.A.R.Othman, Basri, A new empirical equation for estimating specific surface area of supercapacitor carbon electrode from X-ray diffraction, Adv. Mater. Res. 1108 (2015) 1–7, https://doi.org/10.4028/www.scientific.net/AMR.1108.1.

[52] E. Elaiyappillai, R. Srinivasan, Y. Johnbosco, P. Devakumar, K. Murugesan, K. Kesavan, P.M. Johnson, Low cost activated carbon derived from Cucumis Melo fruit peel for electrochemical supercapacitor application, Appl. Surf. Sci. 486 (2019) 527–538, https://doi.org/10.1016/j.apsusc.2019.05.004.

[53] V.S. Bhat, P. Kanagavalli, G. Sriram, RPB, N.S. John, M. Veerapandian, M. Kurkuri, G. Hegde, Low cost, catalyst free, high performance supercapacitors based on porous nano carbon derived from agriculture waste, J. Energy Storage 32 (2020) 101829, https://doi.org/10.1016/j.est.2020.101829.

[54] Y.J. Zhang, Z.J. Xing, Z.K. Duan, M. Li, Y. Wang, Effects of steam activation on the pore structure and surface chemistry of activated carbon derived from bamboo waste, Appl. Surf. Sci. 315 (2014) 279–286, https://doi.org/10.1016/j.apsusc.2014.07.126.

[55] M. Changmai, P. Banerjee, K. Nahar, M.K. Purkait, A novel adsorbent from carrot, tomato and polyethylene terephthalate waste as a potential adsorbent for co (II) from aqueous solution: kinetic and equilibrium studies, J. Environ. Chem. Eng. 6 (2018) 246–257, https://doi.org/10.1016/j.jece.2017.12.009.

[56] T. Qiu, J.G. Yang, X.J. Bai, Y.L. Wang, The preparation of synthetic graphite materials with hierarchical pores from lignite by one-step impregnation and their characterization as dye absorbents, RSC Adv. 9 (2019) 12737–12746, https://doi.org/10.1039/c9ra00343f.

[57] A. Elmouwahidi, E. Bailón-García, A.F. Pérez-Cadenas, F.J. Maldonado-Hódar, F. Carrasco-Marín, Activated carbons from KOH and H3PO4-activation of olive residues and its application as supercapacitor electrodes, Electrochim. Acta 229 (2017) 220–228, https://doi.org/10.1016/j.electacta.2017.01.153.

[58] D. Liu, W. Zhang, W. Huang, Effect of removing silica in rice husk for the preparation of activated carbon for supercapacitor applications, Chin. Chem. Lett. 30 (2019) 1315–1319, https://doi.org/10.1016/j.cclet.2019.02.031.

[59] A. Gopalakrishnan, T.D. Raju, S. Badhulika, Green synthesis of nitrogen, sulfur-co-doped worm-like hierarchical porous carbon derived from ginger for outstanding supercapacitor performance, Carbon N. Y. 168 (2020) 209–219, https://doi.org/10.1016/j.carbon.2020.07.017.

[60] L. Luo, L. Luo, J. Deng, T. Chen, G. Du, M. Fan, W. Zhao, High performance supercapacitor electrodes based on B/N co-doped biomass porous carbon materials by KOH activation and hydrothermal treatment, Int. J. Hydrog. Energy 46 (2021) 31927–31937, https://doi.org/10.1016/j.ijhydene.2021.06.211.

[61] K. Sun, S. Yu, Z. Hu, Z. Li, G. Lei, Q. Xiao, Y. Ding, Oxygen-containing hierarchically porous carbon materials derived from wild jujube pit for high-performance supercapacitor, Electrochim. Acta 231 (2017) 417–428, https://doi.org/10.1016/j.electacta.2017.02.078.

[62] L. Chai, P. Wang, X. Liu, Y. Sun, X. Li, J. Pan, Accurately control the micropore/mesopore ratio to construct a new hierarchical porous carbon with ultrahigh capacitance and rate performance, J. Power Sources 532 (2022), 231324, https://doi.org/10.1016/j.jpowsour.2022.231324.

[63] X. Liang, R. Liu, X. Wu, Biomass waste derived functionalized hierarchical porous carbon with high gravimetric and volumetric capacitances for supercapacitors, Microporous Mesoporous Mater. 310 (2021), 110659, https://doi.org/10.1016/j.micromeso.2020.110659.

[64] A. Jain, M. Ghosh, M. Krajewski, S. Kurungot, M. Michalska, Biomass-derived activated carbon material from native european deciduous trees as an inexpensive and sustainable energy material for supercapacitor application, J. Energy Storage 34 (2021), 102178, https://doi.org/10.1016/j.est.2020.102178.

[65] Z. Zhang, X. An, L. Liu, J. Yang, W. Zhang, H. Dai, H. Cao, Q. Xu, H. Liu, Y. Ni, Chitin nanofibers as versatile bio-templates of zeolitic imidazolate frameworks for N-doped hierarchically porous carbon electrodes for supercapacitor, Carbohydr. Polym. 251 (2021), 117107, https://doi.org/10.1016/j.carbpol.2020.117107.

[66] X.Q. Lin, N. Yang, L. Qiu-Feng, R. Liu, Self-nitrogen-doped porous biocarbon from watermelon rind: a high-performance supercapacitor electrode and its improved electrochemical performance using redox additive electrolyte, Energy Technol. 7 (2019), https://doi.org/10.1002/ente.201800628.

[67] C.K. Roy, S.S. Shah, A.H. Reaz, S. Sultana, A.N. Chowdhury, S.H. Firoz, M.H. Zahir, M.A. Ahmed Qasem, M.A. Aziz, Preparation of hierarchical porous activated carbon from Banana leaves for high-performance supercapacitor: effect of type of electrolytes on performance, Chem. Asian J. 16 (2021) 296–308, https://doi.org/10.1002/asia.202001342.

[68] F. Liu, Z. Wang, H. Zhang, L. Jin, X. Chu, B. Gu, H. Huang, W. Yang, Nitrogen, oxygen and sulfur co-doped hierarchical porous carbons toward high-performance supercapacitors by direct pyrolysis of Kraft lignin, Carbon N. Y. 149 (2019) 105–116, https://doi.org/10.1016/j.carbon.2019.04.023.

[69] C. Zhao, W. Zheng, A review for aqueous electrochemical supercapacitors, Front. Energy Res. 3 (2015) 1–11, https://doi.org/10.3389/fenrg.2015.00023.

[70] M. Sajjad, M.I. Khan, F. Cheng, W. Lu, A review on selection criteria of aqueous electrolytes performance evaluation for advanced asymmetric supercapacitors, J. Energy Storage. 40 (2021), 102729, https://doi.org/10.1016/j.est.2021.102729.

[71] M.D. Liao, C. Peng, S.P. Hou, J. Chen, X.G. Zeng, H.L. Wang, J.H. Lin, Large-scale synthesis of nitrogen-doped activated carbon fibers with high specific surface area for high-performance supercapacitors, Energy Technol. 8 (2020) 1901477, https://doi.org/10.1002/ente.201901477.

[72] B. Pal, S. Yang, S. Ramesh, V. Thangadurai, R. Jose, Electrolyte selection for supercapacitive devices: a critical review, Nanoscale Adv. 1 (2019) 3807–3835, https://doi.org/10.1039/c9na00374f.

[73] S. Sathyamoorthi, P. Chiochan, M. Sawangphruk, High-rate aqueous/ionic liquid dual electrolyte supercapacitor using 3D graphene sponge with an ultrahigh pore volume, Electrochim. Acta 327 (2019), 135014, https://doi.org/10.1016/j.electacta.2019.135014.

[74] M. Jayachandran, A. Rose, T. Maiyalagan, N. Poongodi, T. Vijayakumar, Effect of various aqueous electrolytes on the electrochemical performance of α-MnO2 nanorods as electrode materials for supercapacitor application, Electrochim. Acta 366 (2021), 137412, https://doi.org/10.1016/j.electacta.2020.137412.

[75] R.A. Senthil, V. Yang, J. Pan, Y. Sun, A green and economical approach to derive biomass porous carbon from freely available feather finger grass flower for advanced symmetric supercapacitors, J. Energy Storage 35 (2021), 102287, https://doi.org/10.1016/j.est.2021.102287.

Averrhoa bilimbi leaves-derived oxygen doped 3D-linked hierarchical porous carbon as high-quality electrode material for symmetric supercapacitor

ORIGINALITY REPORT

14%	1%	4%	13%
SIMILARITY INDEX	INTERNET SOURCES	PUBLICATIONS	STUDENT PAPERS

PRIMARY SOURCES

1	Submitted to Universiti Teknologi Malaysia Student Paper	1%
2	Submitted to German University of Technology in Oman Student Paper	1%
3	Submitted to Universidad Estadual Paulista Student Paper	1%
4	Submitted to King Fahd University for Petroleum and Minerals Student Paper	<1%
5	Submitted to Transilvania University of Brasov Student Paper	<1%
6	Submitted to Botswana International University of Science and Technology Student Paper	<1%
7	Submitted to American University in Cairo Student Paper	<1%
	Submitted to University of Birmingham	

8	Student Paper	<1%
9	Submitted to Central University of Himachal Pradesh, Dharamshala Student Paper	<1%
10	Submitted to Chonnam National University Student Paper	<1%
11	Submitted to Technische Universität Clausthal Student Paper	<1%
12	Submitted to Tunghai University Student Paper	<1%
13	Submitted to University of Western Macedonia Student Paper	<1%
14	Submitted to Unviersidad de Granada Student Paper	<1%
15	Submitted to Uva Wellassa University Student Paper	<1%
16	publications.aston.ac.uk Internet Source	<1%
17	Submitted to IIT Delhi Student Paper	<1%
18	Jiang Deng, Tianyi Xiong, Haiyan Wang, Anmin Zheng, Yong Wang. "Effects of Cellulose, Hemicellulose, and Lignin on the Structure	<1%

and Morphology of Porous Carbons", ACS Sustainable Chemistry & Engineering, 2016
Publication

19	Submitted to Virginia Polytechnic Institute and State University Student Paper	<1 %
20	Submitted to Chungnam National University Student Paper	<1 %
21	Submitted to Texas A & M University, Kingville Student Paper	<1 %
22	Submitted to Univerza v Ljubljani Student Paper	<1 %
23	Submitted to Universidad Nacional de Colombia Student Paper	<1 %
24	Submitted to National Science & Technology Development Agency (NSTDA) Student Paper	<1 %
25	Submitted to Indian School of Mines Student Paper	<1 %
26	Submitted to Polytechnic of Turin Student Paper	<1 %
27	Submitted to University of Liverpool Student Paper	<1 %
28	Submitted to VIT University Student Paper	<1 %

29	Rizo Estrada Juan. "Degradación de compuestos organofosforados con nanopartículas hechas a base de cobre", TESIUNAM, 2021 Publication	<1 %
30	Submitted to University of Massachusetts, Lowell Student Paper	<1 %
31	Submitted to NIT Imphal Student Paper	<1 %
32	Submitted to University of Lincoln Student Paper	<1 %
33	Submitted to University of Technology, Sydney Student Paper	<1 %
34	Submitted to Graphic Era University Student Paper	<1 %
35	Submitted to Bogazici University Student Paper	<1 %
36	Byung Chul Lee, Jin Soo Park, Soo Young Jung, Dong Hun Kim, Jung Ho Park, Ho Won Jang, Tae Geun Kim, Seung-Hyub Baek. "Dual-frequency piezoelectric micromachined ultrasound transducer based on polarization switching in ferroelectric thin film", Research Square Platform LLC, 2023 Publication	<1 %

37	Submitted to Escuela Politecnica Nacional Student Paper	<1 %
38	Submitted to University of Sheffield Student Paper	<1 %
39	Submitted to Manchester Metropolitan University Student Paper	<1 %
40	Milena Giulia Gonçalves. "História natural da infecção por variantes genéticas de HPV-16 no canal anal de homens participantes do estudo internacional multicêntrico HIM (HPV Infection in Men)", Universidade de Sao Paulo, Agencia USP de Gestao da Informacao Academica (AGUIA), 2022 Publication	<1 %
41	Submitted to Sungkyunkwan University Student Paper	<1 %
42	Submitted to Edith Cowan University Student Paper	<1 %
43	González Tenorio Diana. "Evaluación de los impactos económicos y ambientales de la producción de biocombustibles líquidos de segunda generación bajo el concepto de biorrefinería", TESIUNAM, 2022 Publication	<1 %
44	Submitted to UC, San Diego	

	Student Paper	<1%
45	Submitted to University of Pretoria Student Paper	<1%
46	Submitted to Zayed University Student Paper	<1%
47	Submitted to Imperial College of Science, Technology and Medicine Student Paper	<1%
48	Submitted to University of Pune Student Paper	<1%
49	Submitted to Visvesvaraya National Institute of Technology Student Paper	<1%
50	Submitted to Gyeongsang National University Student Paper	<1%
51	Submitted to The Robert Gordon University Student Paper	<1%
52	Submitted to University of Durham Student Paper	<1%
53	Submitted to University of Venda Student Paper	<1%
54	Submitted to Vaal University of Technology Student Paper	<1%

55	Xinyi Chia, Alex Yong Sheng Eng, Adriano Ambrosi, Shu Min Tan, Martin Pumera. "Electrochemistry of Nanostructured Layered Transition-Metal Dichalcogenides", Chemical Reviews, 2015 Publication	<1 %
56	Submitted to Visvesvaraya Technological University, Belagavi Student Paper	<1 %
57	Submitted to Nanyang Technological University, Singapore Student Paper	<1 %
58	Submitted to University of Malaya Student Paper	<1 %
59	media.neliti.com Internet Source	<1 %
60	Submitted to Taylor's Education Group Student Paper	<1 %
61	Submitted to Pusan National University Library Student Paper	<1 %
62	Submitted to Universitas Muhammadiyah Surakarta Student Paper	<1 %
63	Zanzottera, Cristina, Aurélie Vicente, Edvige Celasco, Christian Fernandez, Edoardo	<1 %

Garrone, and Barbara Bonelli. "Physico-Chemical Properties of Imogolite Nanotubes Functionalized on Both External and Internal Surfaces", The Journal of Physical Chemistry C, 2012.
Publication

64 Gómez Cruz Juan Manuel. "Development of cost-effective nanoplasmonic-based platforms for portable sensing applications", TESIUNAM, 2021 <1%
Publication

Exclude quotes	Off	Exclude matches	Off
Exclude bibliography	Off		